THE ASTROPHYSICAL JOURNAL, 407:744–751, 1993 April 20

A BROAD-BAND X-RAY TELESCOPE SPECTRUM OF THE MASSIVE X-RAY BINARY X PERSEI

ERIC M. SCHLEGEL,[1,2] PETER J. SERLEMITSOS, KEITH JAHODA, FRANK MARSHALL, ROBERT PETRE, ELIHU BOLDT, RICHARD MUSHOTZKY, JEAN SWANK, ANDREW SZYMKOWIAK, ALAN SMALE,[1,2] AND KIM WEAVER[3]
Code 666, NASA/Goddard Space Flight Center, Greenbelt, MD 20771
Received 1992 August 24; accepted 1992 October 8

ABSTRACT

The *B*road *B*and *X*-*R*ay *T*elescope, covering the 0.3–12 keV bandpass with moderate spectral resolution, observed the Be/X-ray binary X Per in 1990 December during the Astro-1 mission on the space shuttle Columbia. The data obtained are the best to date to search for lines and edges. The data are well fitted by a power-law spectrum with a high-energy cutoff. A low value for the high-energy cutoff is found, implying a slightly weaker magnetic field strength for the X-ray pulsar. No iron line is present at $\sim$6.5 keV with an equivalent width $>$30–40 eV. The BBXRT observation corresponded to the "off" state of X Per's recent "phase change."

Subject headings: stars: emission-line, Be — stars: individual (X Persei) — stars: neutron — X-rays: stars

1. INTRODUCTION

Be stars became known as low-luminosity ($<10^{35}$ ergs s^{-1}) X-ray emitters with the identification of X-ray source 4U 0352+30 with its sixth-magnitude optical counterpart X Per (Braes & Miley 1972; van den Bergh 1972; Brucato & Kristian 1972). Absolute confirmation of the optical identification was established by the $\sim$1″ match between the optical position for X Per and the *Einstein* HRI position of 4U 0352+30 (Weisskopf et al. 1984). The discovery of X-ray pulsations (White et al. 1976) indicated the presence of a compact companion. Subsequent research has shown that these systems are wide binaries, so the neutron star apparently does not influence its Be companion (van den Heuvel & Rappaport 1987). The neutron star can then be used as a probe of the nature of the Be stars themselves, as well as providing information on the system parameters. The pulsars in the Be systems generally are spinning up (in contrast to the rotationally powered pulsars), most likely due to the torque applied by the accreted matter. Thousands of these systems should exist in the Galaxy based upon the number currently known ($\sim$20) and considerations of their evolution and brightness (van den Heuvel & Rappaport 1987). The Be/X-ray binaries are among the most abundant of the X-ray–emitting population. A recent review may be found in Nagase (1989).

X Per itself has been identified as an O9.5 IIIe star (Slettebak 1982) with a degenerate, compact companion, presumably a magnetized neutron star. An orbital period of 580 days has been claimed (Hutchings et al. 1974) but is not definitively confirmed. X-ray pulsations exist at a period of $\sim$835 s (White et al. 1976; Robba & Warwick 1989), believed to be the spin period of the neutron star. This spin period is the longest known for this class of object (van den Heuvel & Rappaport 1987), and for the past 6 years, a net spin-down mode has existed (Robba, Warwick, & Murakami 1992). Early X-ray spectral observations modeled the X Per spectrum as thermal bremsstrahlung radiation from an optically thin plasma at temperatures in the 7–12 keV range (Becker et al. 1979; White et al. 1976; White et al. 1982). The puzzle is that no iron line at $\sim$6.5 keV has ever been detected, when it clearly should have been seen if the above model for the X-ray emission were correct. More recent measurements, made with instruments with better spectral response and resolution (*Tenma*, *Ginga*), have found the data are better fitted by a power-law plus a high-energy cutoff (e.g., Murakami et al. 1987 for *Tenma* data). The power-law spectrum as a model is more typical of X-ray pulsars. What makes X Per unique among the X-ray pulsars is the low value for the high-energy cutoff. Most X-ray pulsars have a high-energy cutoff of $\sim$20–30 keV (White, Swank, & Holt 1983). The value for X Per is more typically $\sim$2–5 keV (to be presented in Table 2). Recently, X Per has undergone a phase change (Norton et al. 1991), and the BBXRT spectrum was obtained approximately in the middle of the low state.

2. THE BBXRT OBSERVATIONS

The Broad Band X-Ray Telescope (Serlemitsos et al. 1992) flew on the shuttle Columbia as one component of the multi-telescope Astro-1 mission. Liftoff occured on 1990 December 2 at 06:49 UT, with a mission duration of approximately 9 days. X Per was observed on day 6.992–7.002 of the mission.

BBXRT was designed and built at GSFC by principal investigator Peter Serlemitsos (Serlemitsos et al. 1992). It consists of two co-aligned telescopes of 3.8 m focal length which cover the 0.3–12 keV band. The mirrors are thin, nested, gold-coated aluminum foils, with an effective area of $\sim$150 cm^2 at 2 keV, and 80 cm^2 at 7 keV for each telescope/detector combination. The mirrors focus the X-rays onto cooled, lithium-drifted silicon, solid state spectrometers. The spectrometers consist of 5 pixels per detector, 512 energy channels per pixel, with the central pixel having a 4′.5 field of view. The overall field of view is 17′. The energy resolution is about 0.09 keV at 1.0 keV, and 0.15 keV at 6 keV. The detector backgrounds are low, with $\sim$0.02 counts s^{-1} in the central pixel, and $\sim$ 0.1 counts s^{-1} in the outer pixels.

X Per was observed for a total of $\sim$870 s centered approximately on day 6.997 of the mission (=UT 1990 December 9

[1] Research Scientist, Universities Space Research Association.
[2] Postal address: Code 668, NASA/Goddard Space Flight Center, Greenbelt MD 20771.
[3] Also University of Maryland.

06:44). Aspect solutions were available at 18 times during the observations, with an RMS error of 9'.1. X Per was observed 1'.9 off-axis which is quite good, given the various pointing problems encountered during the mission. The observation was made during shuttle night, and the nearest Earth limb was dark. The Sun angle was approximately 160° during the observation, the moon angle was approximately 110°, and the Earth angle ranged from about 150° to about 100° during the observation, so there is no bright Earth contamination. Finally, no SAA passage occurred during the observation. An unexplained small "flare" of about 4 s duration at the start of the observation has been explicitly filtered out of the data. The "flare" occurred in several of the outer pixels but was removed from all of the data as a precaution.

While X Per was observed nearly on-axis, the point-spread function of BBXRT is such that approximately 40% of the photons are placed in the outer pixels. We have used the 2 pixels from each telescope containing the majority of the photons. The light curves for each of the pixels are shown in Figure 1, so the reader may judge from Figure 1 the effect of ignoring the pixels left out of the analysis. (Slight gaps in the light curves [particularly the low count rate pixels] are due to guard rate filtering, and indicate non–X-ray particle hits in the detector.) An estimate of the number of photons lost by ignoring the weak pixels may be made as follows. The average count rate (counts s^{-1}) and errors (in the last digit[s]) for each of the pixels are as follows: A0 = 4.28(7); A1 = 1.88(5); A2 = 0.51(3); A3 = 0.19(3); A4 = 0.58(3); B0 = 1.73(5); B1 = 0.26(3); B2 = 0.28(3); B3 = 2.01(4); and B4 = 0.79(4). (Note: the "zero" indicates an on-axis pixel; the other 4 pixels for a given telescope are the outer pixels. There is a rotation between detector A and B of 180° in the numbering scheme.) We then normalize the A0 plus B0 count rate by the summed count rates from all the pixels, yielding a value of ~0.56. When we include the next most "populated" pixels (A1, B3), the normalized value rises to ~0.94. At most then, we ignored ~6% of the data.

An apparent pulse period is visible in the light curve, but just barely, as might be expected for an observation time slightly longer than the known pulse period. No subpulse behavior is evident, based on a power spectrum examination of the data, in spite of the visual appearance of the light curves. The data were divided into energy bands (3.7 to 11 keV, and 1.5 to 3.7 keV, as in Robba & Warwick 1989), and a hardness ratio was generated. No hardening burst behavior similar to that seen in the *EXOSAT* data of Robba & Warwick (1989) (their Fig. 4) was evident. They found a brief hardening burst occurred ~0.07 in phase prior to the pulse minimum. The same behavior was seen in the *Ginga* data (Robba et al. 1992). In addition, the *Ginga* data showed that the hardening pulse is not present on every cycle. Further, the peak of the pulse is ~20% above the mean hardness ratio. It is thus a relatively low-contrast event without considerable data to co-add. The BBXRT data, within the error bars, were consistent with a constant hardness during the observation. An additional hardness ratio was generated, striving for the extremes in the hard versus soft behavior of X Per. This ratio is plotted in Figure 2. Again no hardening bursts are seen. There is a possibility that the phase change (see § 4 below) which occurred in X Per affected the hardness behavior. Alternatively, the BBXRT observation could have coincided with one of the cycles when the hardening pulse was simply not present.

The data were binned such that there were at least 15–20 counts per channel per spectrum. The binning was done objectively, with software that grouped energy channels until the number of counts in the resulting binned channel was at least 15 counts. This binning will produce an "arbitrary" bin size (see, for example, Fig. 3*b* below). The 4 pixels, originally 512 channels each, became ~100 channels each (depending upon the pixel). The first 15 channels of each pixel of the binned data were not included in the fit as they were below the lower level discriminator. The background was an accumulated night background and was generally only a few percent of the signal from X Per (a result of the observation being done under relatively ideal conditions). The response matrix used to fit the spectrum has evolved considerably since the flight (the matrix is known as "test18"), but the vast majority of the changes were made to remove small (~5%–10%) effects. Fits to the Crab yield flat residuals to <5%, and no features exist in the spectrum with an equivalent width >12 eV. The on-axis pixels

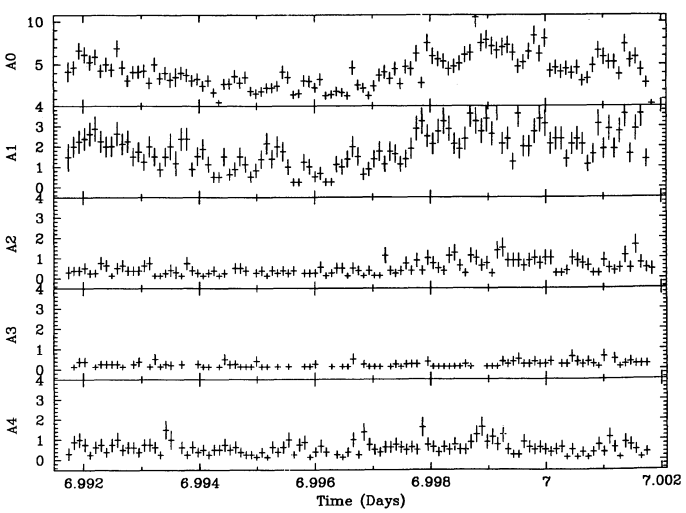

FIG. 1*a*

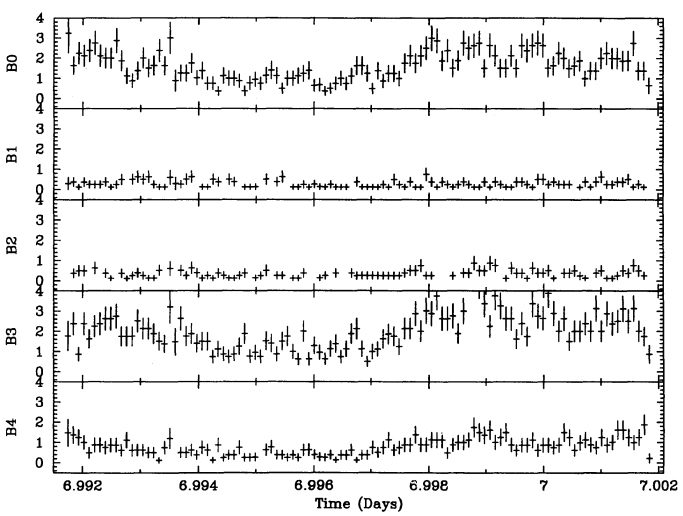

FIG. 1*b*

FIG. 1.—X Per light curves for each BBXRT pixel. Units are counts s^{-1}. Time is in units of days of mission elapsed time. See the text for the correspondence with UT. (*a*) Telescope A; (*b*) telescope B.

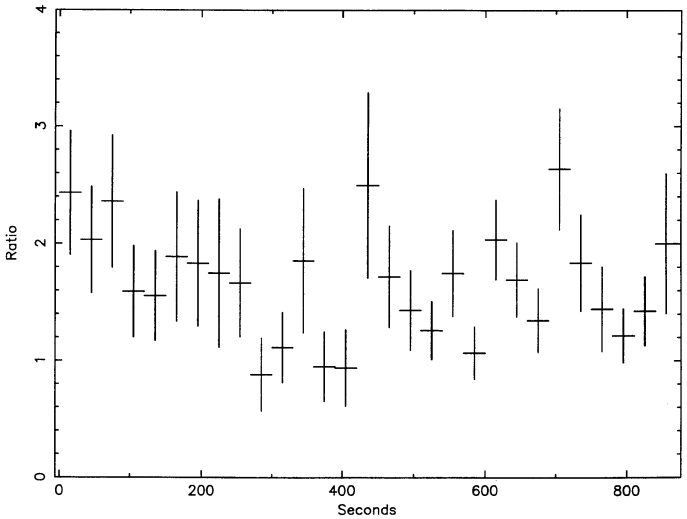

FIG. 2.—The hardness ratio of the BBXRT data summed to 30 s bins. The data are consistent with constant hardness, even during the observed pulse minimum. Energy bands: 3–10 keV/0.65–1.5 keV.

are better calibrated than the off-axis pixels; however, the differences are $\sim <10\%$ and are largely confined to regions below ~ 0.5 keV and above 10 keV. A more detailed discussion of the BBXRT matrix is found in Weaver (1993). Finally, the fitting procedure did a simultaneous fit to the 4 pixels. The normalization parameters varied individually, while the model parameters (power-law index, hydrogen columns, etc.) were freely varied, but forced to be identical among the 4 pixels.

3. THE RESULTS

We turn now to a discussion of the spectrum obtained with BBXRT, and the fitted results. The spectrum obtained is shown in Figure 3*a*, and expanded residuals in the Fe line region are shown in Figure 3*b*. The fitted model is an absorbed power law with a high-energy cutoff. The value for N_H, computed from Gorenstein (1975), for an $E_{B-V} = 0.39 \pm 0.02$ (Fabregat et al. 1992), gives $N_H \sim 2.7 \pm 0.2 \times 10^{21}$ cm^2. This value is identical to within the errors to the formal fitted value from the X-ray spectrum, if all model parameters are free to vary. Formally, we reject simple models (power-law, blackbody, thermal bremsstrahlung) as being inadequate (or producing physically unrealistic parameter values) in describing the data. A broken power-law spectrum provides an acceptable fit; however, to maintain continuity with the historical literature, we use only the power-law spectrum plus high-energy cutoff model. The parameters for the various models are listed in Table 1, and the χ^2 contours for the power-law index and N_H are shown in Figure 4. The unfolded spectrum is presented in Figure 5. The corresponding flux and luminosity are $\sim 4.3 \pm 0.5 \times 10^{-10}$ ergs s^{-1}, and $9^{+8}_{-5} \times 10^{34}$ ergs s^{-1}, for an assumed distance of 1300 ± 400 pc (Fabregat et al. 1992).

We note that the cutoff energy is rather low. Other investigators, for example, Robba & Warwick (1989), have also pointed out the low cutoff energy for X Per. In the accepted model, the cutoff energy is taken to be the value at which the cyclotron resonance absorption becomes strong. Cyclotron absorption lines have been found in several X-ray pulsars (see Nagase 1989 for a review), and the cyclotron lines act as probes of the magnetic field. The implied field strengths are $\sim 10^{12}$ G, with little evidence for field decay, in contrast to theoretical expectation. A correlation appears to exist between the cutoff energy and the cyclotron resonance energy, namely $E_{cyc} \sim 1.4$–$1.8\ E_{cut}$ (Makishima et al. 1992). X Per's value of E_{cut} is approximately 2.24 keV, implying a cyclotron resonance energy of 3–4 keV. We know that the cyclotron resonance occurs at a rest frame energy of $E_{cyc} = 11.6\ (B/10^{12}\ \text{G})$ keV, and by using the apparent correlation to predict the cyclotron energy for X Per, we infer that the magnetic field in the X Per system is slightly weaker ($\sim 0.3 \times 10^{12}$ G) than is typical for X-ray pulsars (1–4×10^{12} G). Only X2259+586 has a comparable cut off energy, yet a cyclotron absorption feature appears to be present at about the expected energy (Koyama et al. 1989; Nagase 1989).

The presence of an iron line is also of interest in this system. The emission line has been attributed to fluorescence from ionized iron, with the line generally found at ~ 6.4 keV (Nagase 1989). The Fe line in X Per has never been seen, so only upper limits to the line equivalent width have been available. Previous missions, with increasingly better energy resolution, have assigned increasingly lower upper limits (e.g., Robba & Warwick 1989). The interpretation of the upper limit on the iron line has been that the emission is not truly thermal in nature (e.g., White et al. 1982 or White et al. 1983). This interpretation fits with that of the X-ray spectral behavior of X-ray pulsars (power law), as opposed to the early spectral fits which used a thermal bremsstrahlung spectrum (e.g., Becker et al. 1979; White et al. 1976). If the emission were thermal, an iron line should be present with an equivalent width of about 200–800 eV (White et al. 1982; White et al. 1983). The best previous upper limit was 60 eV (Robba & Warwick 1989).

Assigning a 90% confidence level to the presence of an Fe line proved difficult. No line is visibly present in any of the spectra, regardless of the energy binning, as was visible in

TABLE 1

FORMAL FITS TO BINNED X PERSEI SPECTRUM

Model	χ^2	χ^2/ν	$N_H(10^{22}$ cm$^{-2})$	Parameter 1[a]	Normalization for Pixel A0	Parameter 2[a]	Parameter 3[a]
Power-law	360.2	1.072	0.45 ± 0.03	1.40 ± 0.03	0.032 ± 0.001		
Bremsstrahlung	343.6	1.023	0.42 ± 0.02	27.99 ± 4.64	0.0096 ± 0.0069		
Blackbody	570.0	1.696	0.0 ± 0.04	1.13 ± 0.02	0.0023 ± 0.0001		
Raymond plasma	343.5	1.022	0.42 ± 0.02	27.91 ± 5.16	0.169 ± 0.004		
Broken power-law	323.7	0.969	0.26 ± 0.04	0.81 ± 0.13	0.0196 ± 0.0020	2.62 ± 0.18	1.56 ± 0.05
Power law + high E_{cut}	315.0	0.943	0.25 ± 0.04	0.79 ± 0.15	0.0193 ± 0.0021	2.24 ± 0.37	6.08 ± 1.22

[a] Parameter 1 is kT or index, depending upon the model; parameters 2 and 3 are model-dependent: for the broken power law, the parameters are the break energy, and the second index, respectively; for the high-energy cutoff, the parameters are the cutoff energy and the fold energy, respectively. The original number of degrees of freedom, for all models, was 342. The number of model parameters, available by counting the parameters in the above table, must be subtracted. The normalizations for pixels A1, B0, and B3 are not listed, but are approximately 0.41, 0.39, and 0.45 of the A0 value.

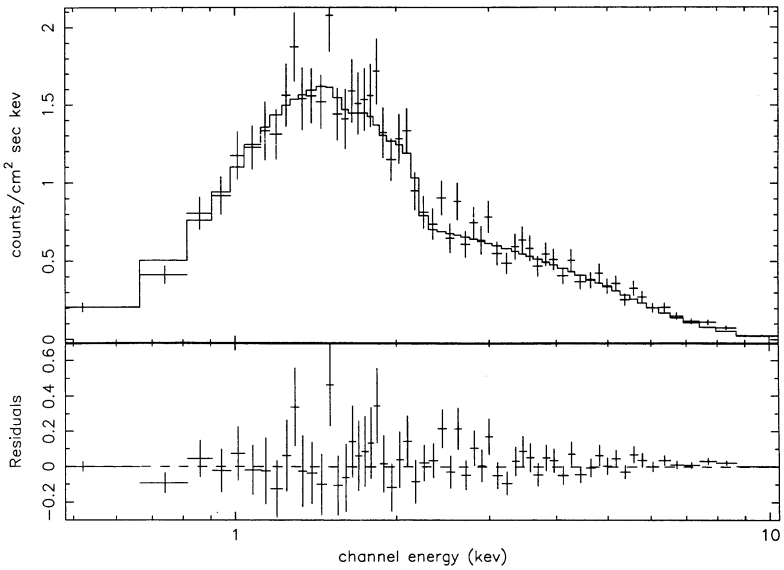

FIG. 3*a*

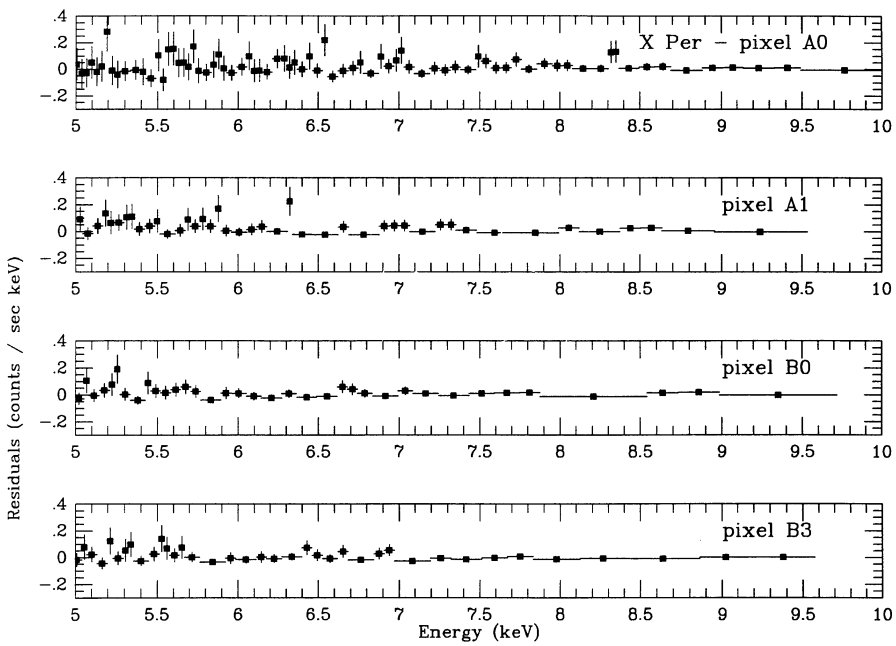

FIG. 3*b*

FIG. 3.—(*a*) The fitted X Per BBXRT spectrum, using photons from pixels A0, A1, B0, and B3. The model is an absorbed power law with high-energy cutoff. The plot shows only the fit to pixel A0, as the others differ only in the normalization value. (*b*) An expansion of (*a*) in the Fe line region showing the residuals for all four pixels.

Figure 3*b* and in Figure 6*a*, where the data divided by the best-fit continuum model are shown. Fits of a Gaussian were attempted at various energies and line widths at which Fe emission might be expected (6.4–6.9 keV, $\sigma \sim 10$–200 eV). No fit was robustly successful until the Gaussian width was below $\sim$20 eV. These fits were clearly fits to noise in the data. A formal upper limit can, however, be assigned in the following manner. The power-law continuum model parameters were frozen at their minimum values, and a Gaussian component was added. Values of the Gaussian line energy were stepped from 6.0 keV to 7.1 keV in steps of 0.1 keV, and values of the line width were stepped from 0.01 keV to 0.09 keV in steps of 0.01 keV, with additional grid points at 0.15 and 0.20 keV, and an equivalent width was determined at each grid location as follows. The relative normalization of the Gaussian component for the 4 pixels were fixed at their corresponding ratios for the continuum normalizations. The absolute normalization of the Gaussian component was then increased until χ^2 changed by +2.71, the value corresponding to the 90% contour for one parameter of interest, and the equivalent width was computed. Representative results are plotted in Figure 6*b*. Note that the best previous limit was 60 eV (Robba & Warwick 1989). The

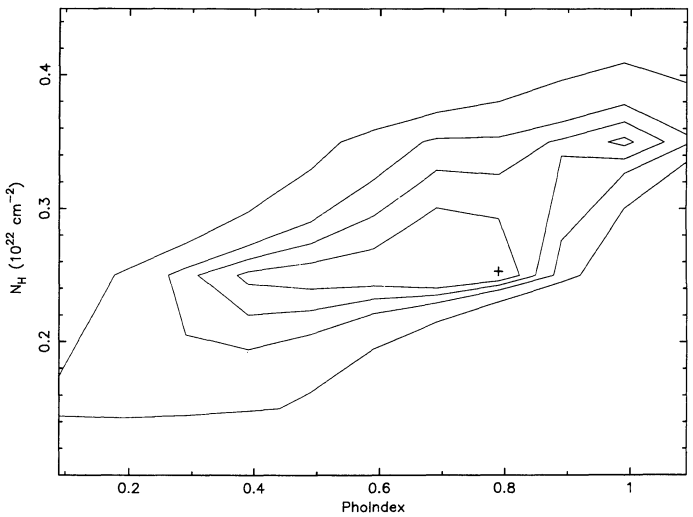

FIG. 4.—The χ^2 contours for the fitted values of N_H and the power-law index. The contours are shown at $\delta\chi^2$ levels of 1.0 (68.3% = 1 σ for one parameter), 2.71 (90% for one parameter), 4.61 (90% for two parameters, and 9.21 (99% for two parameters).

upper limit on the equivalent width is now a function of the line width at a particular line energy. For Fe lines at the usual locations (6.39, 6.64, 6.93 keV), we see that the upper limit varies from ~50 to ~30 to ~60 eV. More counts per bin will be necessary to constrain better the equivalent width and energy of a line in this energy region. One benefit of Figure 6*b* is that the reader can self-judge the presence or absence of an iron line in this region.

Some specific behavior of the upper limit curves in Figure 6*b* is not completely understood. The "linelike" behavior around 6.3 keV is the most puzzling. These peaks are robust, as additional grid points were examined using the procedure described above. The additional points were incremented by 0.02 keV from 6.20 to 6.40 keV. This process (not presented) yields a smooth version of Figure 6*b* in the 6.3 keV region, and not a "spike" as might be expected from a channel value randomly scattering high. The observed behavior of Figure 6*b* prompted a return to the line-fitting program, specifically aiming to place a line in this region. Such a line fit did not converge to a solution, the fits invariably producing a zero-width line, and usually producing a zero normalization value. We conclude that, if there are lines in this region, then only a higher resolution instrument, or a longer exposure time, will detect them. Most likely, the "peak" is due to statistically high channels, as can be seen by examining Figure 6*a*. The "linelike" behavior near 7.0 keV is most likely due to the declining number of photons beyond 7 keV, so that the upper limit curve becomes more noisy. The small rise at ~6.7 keV for a small line widths suggests that a narrow line may exist at these energies, although a mere statistical fluctuation at that energy would mimic the presence of a line.

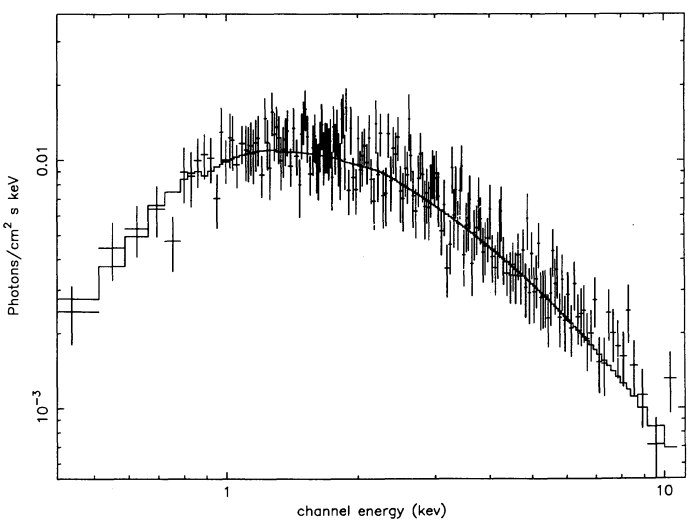

FIG. 5.—The unfolded spectrum of X Per

We have also examined the data for the presence of the iron edge at ~7.1 keV. The exact edge energy depends upon the ionization state, so a wide range was permitted for the edge energy. The edge fit was done by freezing the power-law parameters, allowing only the edge normalization, the edge position, and edge optical depth to vary. Figure 7 shows the upper limit on the edge's presence. The 90% confidence contour is consistent with zero optical depth for the edge. The upper limit on the edge implies that little or no material is physically near the X Per system on a direct line-of-sight to the system.

4. DISCUSSION

X Per has recently undergone a phase change (Norton et al. 1991; Reynolds et al. 1992). The Hα line was in absorption during the Astro-1 flight but was in emission at least as late as 1990 February 21 (Reynolds et al. 1992). By 1990 September, the Hα line was in absorption. This behavior is consistent with the disappearance of the circumstellar material in the X Per system, in which the Be star characteristics revert to those of an ordinary B star. The emission-line disappearance behavior is rather typical of Be stars (see, for example, Slettebak & Reynolds 1978) but is *not* typical of the Be/X-ray binaries. Only two systems exhibiting the emission-line behavior are known: GX 304−1 (Corbet et al. 1986) and X Per. γ Cas (Jernigan 1976; White et al. 1982) would join this group if evidence for binarity could be conclusively established. The immediate question is whether the known optical/infrared phase change correlates with the X-ray spectrum.

X Per has been observed with many previous X-ray missions. Table 2 lists the fitted parameters from these observations; Figure 8*a* shows the plotted values of N_H, if it is permitted to be a variable in the spectral fits, while Figure 8*b* shows the photon power-law index as a function of time. Note that the early models were a simple, absorbed power-law, while the model used for missions from *EXOSAT* to BBXRT is an absorbed power-law plus a high-energy cutoff. The BBXRT value of the power-law index is rather tightly constrained. Comparing the BBXRT value with the values measured by other missions, it is clear that the power-law index varies with time and is possibly correlated with the known phase changes. A fit to the *Ginga* data obtained in 1990 January (Robba et al. 1992) yielded a value of 1.8 ± 0.16 for the photon index. This is relatively steep and perhaps indicates the date of the phase change when the X-ray pulsar was more directly observable.

Does a correlation exist between the optical/infrared and the X-ray observations? In Figures 8*a* and 8*b*, the optical faint state points have been shaded. It is unfortunately clear that there is no discernible pattern, such as high N_H in a faint state. It must be remembered, however, that the phase change itself is

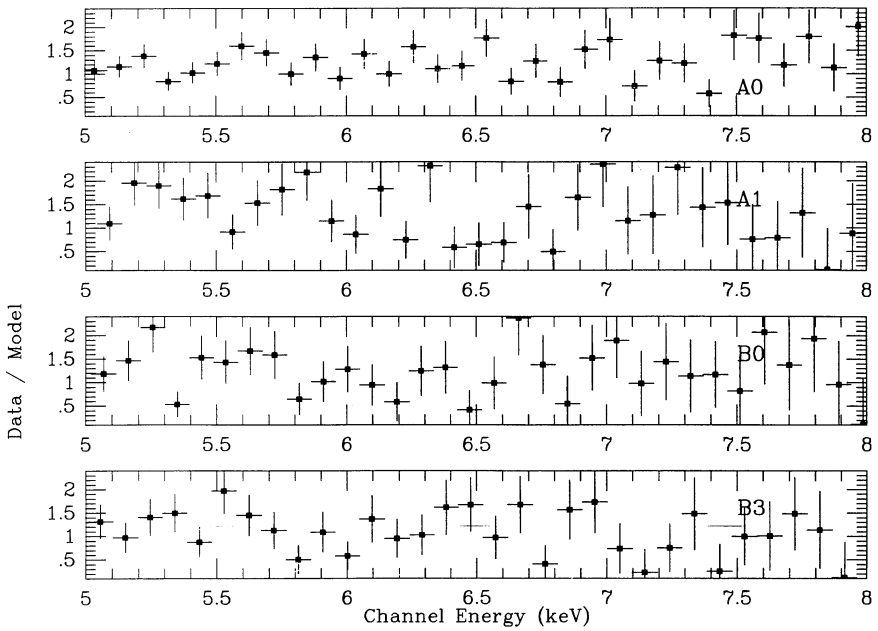

FIG. 6a

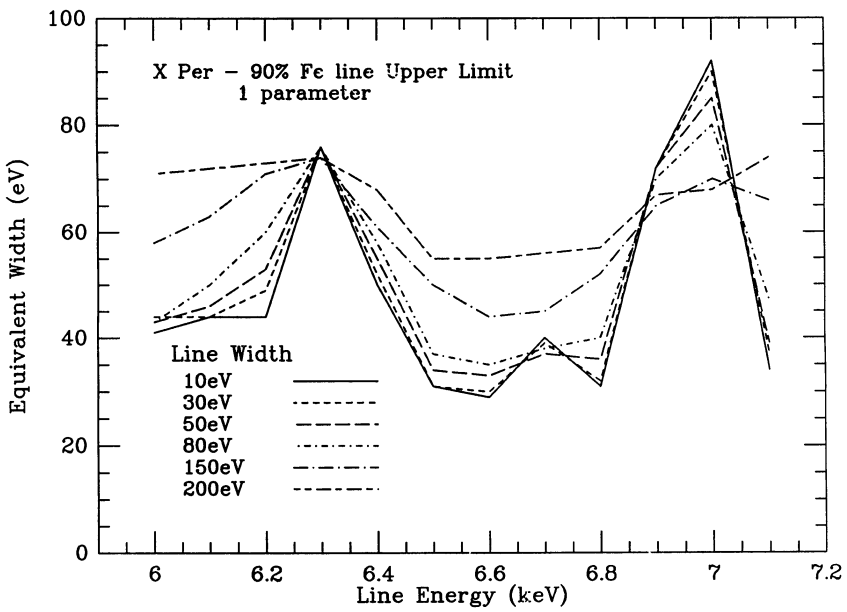

FIG. 6b

FIG. 6.—(*a*) The data divided by the best-fit continuum model. Each pixel is shown (from top, A0, A1, B0, B3). It is clear that there is an upper limit on the presence of an Fe line under assumption that the line appears in all pixels. (*b*) The upper limit on the presence of an iron line. See the description in the text on the production of this figure.

a relatively brief affair, so that the observations summarized here may not be sufficiently well sampled to answer the question definitively. Further, the variation in N_H is not surprising, given that the Be companion emits a wind which, for typical accretion efficiencies, will likely leave considerable unaccreted material bound to the system. White et al. (1983) point out that variations of up to $\sim 10^{23}$ H cm^{-2} have been seen and are usually seen at a particular orbital phase. That the value of N_H measured by BBXRT matches the optically determined E_{B-V} during a known faint state suggests that the extra absorbing material normally surrounding X Per had dissipated. Finally, the variation in the photon power-law index is more puzzling, but only a greater density of observations, X-ray and optical/infrared, will be able to address the nature of the variation. Unfortunately, since no definitive orbital period is known, no orbital phases can be assigned, and no investigation of phase-related behavior is possible. We can not separate phase-related changes from state-related changes. It is thus critical for any study of X Per to establish conclusively the orbital period for the system. A step has been taken by Stickland (1992) and Reynolds et al. (1992), who claim there is no variation above a few km s^{-1} based upon a differential velocity analysis of the

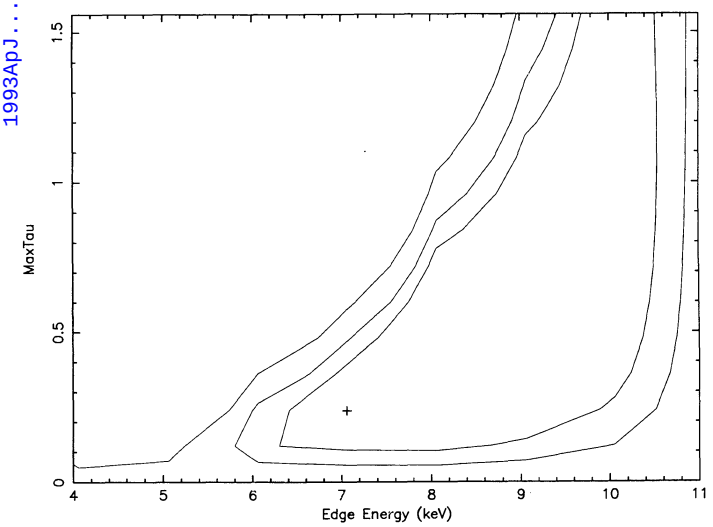

FIG. 7.—The upper limit on the presence of an iron edge as a function of the edge energy. "MaxTau" represents the absorption depth at the threshold energy.

IUE spectra obtained on X Per (Stickland), and a recent, 2-year optical spectroscopic study (Reynolds et al.). Stickland rules out a massive black hole companion, but the limits are insufficient to rule out a neutron star. Reynolds et al. do not confirm the 580 day period, but do suggest that X Per is a velocity variable.

The high-energy cutoff has been thought to be cyclotron absorption. Recent discoveries of cyclotron absorption features have reinforced the interpretation that the cyclotron resonance feature accounts for the turnover in the continuum (see, for example, Mihara et al. 1991). We note that the cutoff energy for X Per is quite low ($E_{cut} \sim 2.3$ keV) in comparison with other X-ray pulsars ($E_{cut} \sim 20$ keV). As Tanaka (1986) has pointed out, if the high-energy cutoff is thermal in origin, then the fold energy E_F will typically be about 0.3 of E_{cut}, implying a cutoff sharper than is expected for a thermal origin. Cyclotron absorption features have been found in those X-ray pulsars with the sharpest cutoffs (White et al. 1983). For approximately 5 of the known X-ray pulsars, E_F is often considerably smaller than 0.3 of E_{cut}, and approaches 10% of E_{cut} for three systems (Her X-1, X1538−52, X1626−67). The continuum fits to the X Per data show an E_F larger than E_{cut} by a factor of about 3, which apparently occurs in only one other system (X1657−41) (Tanaka 1986). This implies that the cyclotron resonance absorption is not as strong in X Per as in other X-ray pulsars. Of note is the observation (White et al. 1983) that the sharpest high-energy cutoffs occur at a luminosity of about 4×10^{37} ergs s^{-1}. The luminosity of X Per is $\sim 10^{35}$ ergs s^{-1}, a factor of about 400 lower. A cyclotron absorption feature may then not be expected. It is perhaps possible that X Per represents a low magnetic field analog of the more typical X-ray pulsar. Further discoveries of such systems would support such an interpretation, as such objects may be difficult to detect or recognize (Makishima et al. 1990). However, we do note that the cyclotron absorption feature may be of sufficiently low contrast that only higher quality data will reveal it.

In summary, the most important result of the BBXRT observation of X Per is the upper limit on the iron line equivalent width at ~6.5 keV. The upper limit has dropped from the early limit of 200 eV (Becker et al. 1979) to the BBXRT value of ~30–40 eV. The BBXRT observation has essentially eliminated any possibility that the X-ray spectrum of X Per contains a thermal component. The low value of the high-energy cutoff suggests that X Per is an analog of the more typical X-ray pulsars. The BBXRT data do indicate the need for greater X-ray sampling of systems such as X Per to understand the changes in the power-law index as a function of time.

TABLE 2

PREVIOUS X PERSEI POWER-LAW SPECTRAL FIT PARAMETERS

Date	MJD	$N_H(10^{22}$ cm$^{-2})$	PLI[a]	E_C[b]	E_F[c]	Flux[d]	χ^2	DOF[e]	Mission[f]	References
1972 Dec 22	41673.5	1.1 ± 0.4	1.1 ± 0.3	...	...	...	...	...	C	1
1972 Dec 22	41673.5	0.5 ± 0.1	1.16 ± 0.16	...	...	...	...	...	C	1
1975 Jan 10	42422.5	< 10. ± 2.20	0.50	...	...	...	...	...	C	1
1975 Aug	42630.	2.4 ± 0.5	1.85 ± 0.10	...	...	...	...	...	A	1
1978 Aug 22	43742.5	2.5	1.	...	...	...	58	35	2	2
1983 Dec 22	45690.5	< 2.	0.62 ± 0.44	2.7 ± 0.7	4.6 ± 1.6	1.5	39	43	E	3
1984 Jan 9	45708.5	< 2.	0.79 ± 0.24	3.2 ± 0.4	4.5 ± 0.8	1.4	29	43	E	3
1984 Jan 10	45709.5	< 2.	1.2 ± 1.2	2.8 ± 1.1	< 10.	1.2	36	43	E	3
1984 Jan 25	45724.5	1.3 ± 1.0	1.61 ± 0.38	5.5 ± 2.0	< 9.	1.3	36	43	E	3
1984 Feb 24	45754.5	< 2.	0.9 ± 1.2	3.1 ± 0.9	< 7.	1.6	55	43	E	3
1984 Nov 11	46015.5	2.51 ± 1.58	1.7 ± 0.3	6.7 ± 1.0	4.0 ± 1.6	2 ± 1	24	26	T	4
1986 Feb 11	46472.5	0.93 ± 0.48	1.40 ± 0.28	4.1 ± 1.4	19. ± 13.	2.2	50	42	E	3
1986 Feb 12	46473.5	< 0.14	1.05 ± 0.10	4.8 ± 0.9	13.5 ± 4.8	2.9	44	41	E	3
1986 Feb 13	46474.5	0.57 ± 0.16	1.26 ± 0.08	4.8 ± 0.3	7.3 ± 1.4	2.5	49	42	E	3
1990 Jan 28	47919.5	1.9 ± 0.65	1.8 ± 0.16	6.2 ± 0.75	9.39 ± 0.1	...	...	...	G	5
1990 Dec 9	48234.8	0.25 ± 0.04	0.79 ± 0.25	2.24 ± 0.37	6.08 ± 1.21	4.27 ± 0.46	315.0	342	B	

NOTE.—Error values are 90% confidence values.

[a] Photon Power-law Index.

[b] Cutoff energy (keV).

[c] Fold energy in keV.

[d] 2–10 keV flux (units = 10^{-10} ergs s^{-1} cm^{-2}).

[e] Degrees of freedom.

[f] Mission: A = *Ariel V*, B = BBXRT, C = *Copernicus*, E = *EXOSAT*, G = *Ginga*, T = *Tenma*, 2 = *HEAO 1* A-2. The BBXRT data used all 4 pixels as described in the text.

REFERENCES.—(1) White et al. 1976; (2) White et al. 1982; (3) Robba & Warwick 1989; (4) Murakami et al. 1987; (5) Robba, Warwick, & Murakami 1992.

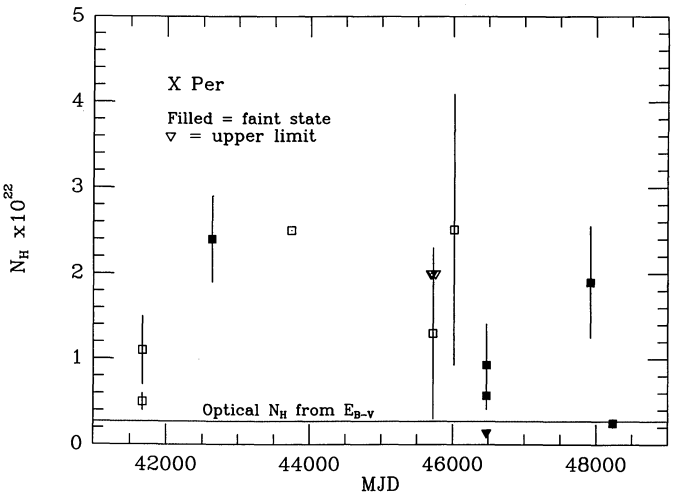

FIG. 8*a*

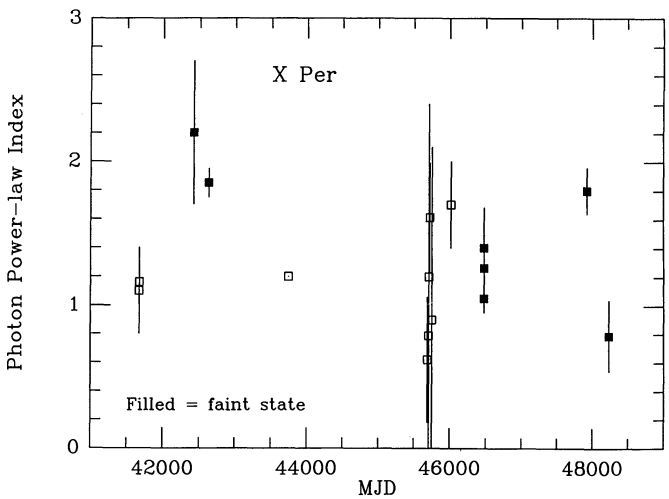

FIG. 8*b*

FIG. 8.—The values of (*a*) N_H, and (*b*) the power-law index, as a function of time for all measurements of N_H and the power-law index for X Per from previous X-ray missions. The missions may be identified with the aid of Table 2. A quick listing, for the points on the power-law graph, is (*left to right*) *Copernicus* (three points), *Ariel V*, *HEAO 1 A-2* (with no error bar), *EXOSAT* (the thin, vertical cloud), *Tenma* (single point at ~46,000), *EXOSAT* (three points), *Ginga*, and BBXRT. Recall that the model used changes from an absorbed power law to an absorbed power law with an high-energy cutoff starting with the *EXOSAT* points.

REFERENCES

Becker, R. H., Boldt, E. A., Holt, S. S., Pravdo, S. H., Robinson-Saba, J., Serlemitsos, P. J., & Swank, J. H. 1979, ApJ, 227, L21.
Braes, L. L. E., & Miley, G. K. 1972, Nature, 235, 273
Brucato, R. J., & Kristian, J. 1972, ApJ, 173, L105
Corbet, R. H. D., Smale, A. P., Menzies, J. W., Branduardi-Raymont, G., Charles, P. A., Mason, K. O., & Boothe, L. 1986, MNRAS, 221, 961
Fabregat, J., et al. 1992, A&A, 259, 522
Gorenstein, P. 1975, ApJ, 198, 95
Hutchings, J. B., Cowley, A. P., Crampton, D., & Redman, R. O. 1974, ApJ, 191, L101
Jernigan, J. 1976, IAU Circ., 2900
Koyama, K., et al. 1989, PASJ, 41, 461
Makishima, K., et al. 1990, ApJ, 365, L59
Makishima, K., Mihara, T., Nagase, F., & Murakami, T. 1992, in Proc. 28th Yamada Conference on X-Ray Astronomy, ed. Y. Tanaka & K. Koyama (Tokyo: Universal Academy), 23
Mihara, T., Makishima, K., Kamijo, S., Ohashi, T., Nagase, F., Tanaka, Y., & Koyama, K. 1991, ApJ, 379, L61
Murakami, T., Ikegami, T., Inoue, H., & Makishima, K. 1987, PASJ, 39, 253
Nagase, F. 1989, PASJ, 41, 1
Norton, A. J., et al. 1991, MNRAS, 253, 579
Reynolds, A. P., Hilditch, R. W., Bell, S. A., Pollacco, D. L., & Edwin, R. P. 1992, MNRAS, 258, 439
Robba, N. R., & Warwick, R. S. 1989, ApJ, 346, 469
Robba, N. R., Warwick, R. S., & Murakami, T. 1992, in Proc. of the 28th Yamada Conference on X-Ray Astronomy, ed. Y. Tanaka & K. Koyama (Tokyo: Universal Academy), 93
Serlemitsos, P. J., et al. 1992, in Proc. of the 28th Yamada Conference on X-Ray Astronomy, ed. Y. Tanaka & K. Koyama (Tokyo: Universal Academy), 221
Slettebak, A. 1982, ApJS, 50, 55
Slettebak, A., & Reynolds, R. C. 1978, ApJS, 38, 205
Stickland, D. J. 1992, MNRAS, 257, 21P
Tanaka, Y. 1986, in Radiation Hydrodynamics in Stars and Compact Objects, ed. D. Mihalas & K.-H. Winkler (Berlin: Springer-Verlag), 198
van den Bergh, S. 1972, Nature, 235, 273
van den Heuvel, E., & Rappaport, S. 1987, in Physics of Be Stars, ed. A. Slettebak & T. Snow (Cambridge: Cambridge Univ. Press), 291
Weaver, K. A. 1993, Ph.D. thesis, Univ. of Maryland, in preparation
Weisskopf, M., et al. 1984, ApJ, 278, 711
White, N. E., Mason, K. O., Sanford, P. W., & Murdin, P. 1976, MNRAS, 176, 201
White, N. E., Swank, J. H., & Holt, S. S. 1983, ApJ, 270, 711
White, N. E., Swank, J. H., Holt, S. S., & Parmar, A. N. 1982, ApJ, 263, 277